A Novel Blind Spectral Unmixing Method Based on Error Analysis of Linear Mixture Model

Chunzhi Li, Faming Fang, Aimin Zhou, and Guixu Zhang

***Abstract*—It is well known that the *linear mixture model (LMM)* is attracting much attention due to its simplicity. However, some theoretical analysis reveals that the traditional LMM also impedes the improvement of blind *spectral unmixing*. For this reason, we propose a *novel blind spectral unmixing method (NBSUM)* in this letter. NBSUM utilizes the *conjugate gradient* to calculate end-member spectral and abundance, which can not only overcome some shortcomings of the traditional LMM but also provide more accurate results. NBSUM is compared with some state-of-the-art approaches on both synthetic and real hyperspectral data sets, and the experimental results demonstrate the efficacy of the proposed method.**

***Index Terms*—Benign equation, blind spectral unmixing (SU), error analysis, linear mixture model (LMM), novel blind spectral unmixing method (NBSUM).**

I. Introduction

SPECTRAL unmixing (SU) aims to decompose mixed pixels into a set of constituent spectra (end-members) and their corresponding proportions (abundances). In SU, the *linear mixture model (LMM)* and *nonlinear mixture model (NLMM)* have been widely used [1]. In spectra, the virtual end-members formed by the interactive term can highly correlate with the true end-members [2], which may lead to a serious collinearity problem in NLMM. Therefore, this letter focuses on LMM, which assumes that each mixed pixel is a linear combination of some end-members. Over the past years, various constraints have been imposed on LMM to enhance its capability in subpixel detection and mixed-pixel classification and quantification. All such extensions attempt to increase and enhance their linear unmixing ability [3]. Usually, the methods based on LMM can be classified into the geometrical and statistical approaches [3]. Comparing to the geometrical approaches, the statistical approaches are more suitable for highly mixed spectra [4].

The *nonnegative matrix factorization (NMF)* is a typical statistical approach for *blind source separation (BSS)* [5]. Since both the spectral end-member and abundance matrices are unknown, a SU problem becomes a BSS problem or a blind SU problem, and NMF has been widely used. By decomposing a set of high-dimensional data into two nonnegative matrices, NMF can overcome some disadvantages of geometric approaches. In the case of blind SU, NMF can find basis vectors for the LMM. The major challenges faced by NMF are as follows: 1) the solution space is usually neither sparse nor uniqueness, and 2) there usually exists a large amount of local minima [6]. To overcome these shortcomings, it is natural to introduce additional auxiliary constraints into the NMF model with the characteristics of different applications. This idea is followed by some methods, such as NMF based on minimum volume constraint (NMF-MVC) [7], $L_{1/2}$NMF [6], Abundance Separation and Smoothness Constrained NMF (ASSNMF) [8], and by using the S-measure constraint (SMC), a gradient-based sparse NMF (NMF-SMC) [9]. Although these methods can improve SU performance greatly, they still suffer from collinearity effect [2], and the estimates of end-member fraction may be affected erratically in response to minor changes in noise level in the matrix deconvolution process. A major cause of limitations might be that, in blind SU, the NMF is based on LMM.

To deal with the problems faced by NMF on blind SU, this letter proposes a *novel blind spectral unmixing method (NBSUM)* by the error analysis of LMM. In NBSUM, the *conjugate gradient (CG)* is employed to realize blind SU.

II. Error Analysis of Traditional LMM

LMM assumes that end-members do not interfere with each other [10] and can be formulated as

$$X = WH + \xi \tag{1}$$

where $X = [x_1^T, x_2^T, \ldots, x_M^T]^T \in \Re^{M\times N}$ denotes the collected mixtures, $W \in \Re^{M\times K}$ denotes the end-member spectra matrix, and $H \in \Re^{K\times N}$ is the weighted matrix which denotes the corresponding abundances. Based on the real background, each column of H is summed to one. M, K, and N denote the number of bands in end-member signatures, the number of end-members, and the number of pixels in the hyperspectral remote sensing image, respectively. $\xi \in \Re^{M\times N}$ is the random measurement error matrix. In (1), W, H, and X are all required to be nonnegative.

In blind SU, NMF is employed to find two nonnegative matrices W and H by using the projected *alternating least squares estimation (ALSE)*. Hereafter, we assume that the random measurement errors ξ are brought about alternately. Consequently, when fixing W to find H, ξ stems from Δ_W and can be expressed as

$$\xi = \Delta_W H \tag{2}$$

Manuscript received July 22, 2013; revised September 22, 2013; accepted October 9, 2013. Date of publication December 11, 2013; date of current version March 11, 2014. This work was supported in part by the National Basic Research Program of China under Grant 2011CB707104 and in part by the National Natural Science Foundation of China under Grants 61372147 and 61273313.

C. Li is with the Department of Computer Science and Technology, East China Normal University, Shanghai 200241, China, and also with the Huzhou Teachers College, Huzhou 31300, China.

F. Fang and A. Zhou are with the Department of Computer Science, East China Normal University, Shanghai 200241, China.

G. Zhang is with the Department of Computer Science and Key Laboratory of Geographic Information Science, Ministry of Education, East China Normal University, Shanghai 200241, China (e-mail: gxzhang@cs.ecnu.edu.cn).

Color versions of one or more of the figures in this paper are available online at http://ieeexplore.ieee.org.

Digital Object Identifier 10.1109/LGRS.2013.2285926

where Δ_W denotes the difference between the library end-member spectra and the true end-member spectra constituting mixed pixels. Moreover, when fixing H to find W, ξ can be expressed as

$$\xi = W\Delta_H \tag{3}$$

where Δ_H is the difference between the real end-member abundance and the calculated end-member abundance.

In the following, we consider how to find the end-member abundance matrix H with a fixed end-member matrix W. Let $\xi = \Delta_W H$, and H can be derived from (1) as

$$H_{NMF} = (W^T W)^{-1} W^T X. \tag{4}$$

It has been shown that, if the end-member spectra are linearly independent, $(W^T W)^{-1}$ always exists [11].

To evaluate the effect of the traditional LMM on the estimation of H, a criterion of *mean square error (mse)* is used. Define Ψ_H [11] as

$$\Psi_H = E\left[\frac{\zeta_H^T \zeta_H}{K}\right] \tag{5}$$

where $\zeta_H = H_{NMF} - \widehat{H}$ denotes the error of abundance estimation, $\widehat{H}$ is the real end-member abundance matrix, and $E[\cdot]$ calculates the expectation value of a random variable. It is known that the sum of the eigenvalues of a matrix is the mean of the energy. Therefore, (5) can be further derived as [11]

$$\Psi_H = \frac{1}{K} E\left[Tr\left[\zeta_H^T \zeta_H\right]\right] \tag{6}$$

where $Tr[\cdot]$ is the trace of a matrix. Let $U = (W^T W)^{-1} W^T$ be the pseudoinverse of the matrix W. Substituting (4) into (6), we can get

$$\Psi_H = \frac{1}{K} E\left[Tr\left[(UX - \widehat{H})^T (UX - \widehat{H})\right]\right]. \tag{7}$$

According to (1) and (2), X can be written as

$$X = W\widehat{H} + \Delta_W H. \tag{8}$$

For any given two matrices F and C, there exists $Tr(FC) = Tr(CF)$. Utilizing this matrix property and substituting (8) into (7), we can get

$$\Psi_H = \frac{1}{K} Tr[\xi \xi^T U^T U]. \tag{9}$$

To achieve an accurate estimation of H, Ψ_H needs to be minimized. Since K is a given constant, the term of $Tr[\xi\xi^T U^T U]$ needs be optimized. It should be noted that the term of $Tr[\xi\xi^T U^T U]$ is not only related to ξ (i.e., the random measurement error matrix of LMM) but also related to U. However, the traditional LMM only minimizes ξ as in (1).

As the same in the above, we can find the end-member matrix W with a fixed end-member abundance matrix H. The mse of end-member spectral matrix W, Ψ_W, can be derived as

$$\Psi_W = \frac{1}{K} Tr[\xi \xi^T V^T V] \tag{10}$$

where V is the pseudoinverse of the matrix H. It is obvious that it required to minimize the term $Tr[\xi\xi^T V^T V]$ to get a more accurate W. Unfortunately, the traditional LMM does not consider V in practice.

In order to get accurate results, traditional blind SU methods usually utilize sparse NMF to control overfitting and add a sparseness regularization term to improve the uniqueness of the decomposition [4], [12]. In these methods, the error function to be minimized is usually defined as

$$D(W,H) = \frac{1}{2}\|X - WH\|_F^2 + \lambda \|H\|_q \qquad 0 < q \leq 2 \tag{11}$$

where λ is a regularization parameter and $\|H\|_q$ is the regularization term.

In traditional blind SU methods, the sparsity constraint can improve the accuracy of the result. However, the additional auxiliary constraints may also lead to unstable and local optimal results. Generally speaking, the L_0 regularizer considers the number of nonzero elements in an abundance matrix and yields the most sparse result for a given cost function. However, the solution of the L_0 regularizer is an NP-hard optimization problem that cannot be solved in practice.

III. NBSUM

This section presents the details of the proposed NBSUM for blind SU. In NBSUM, the ALSE method is used to calculate the nonnegative matrices W and H iteratively.

First, we fix W to find H. According to the error analysis of the traditional LMM, the accuracy of H is affected by ξ and U. Therefore, we can obtain H from the following model:

$$X = WH + U^T \xi. \tag{12}$$

Second, we fix H to find W. As the same in (12), we can deduce the following model by taking consideration of (10):

$$X^T = H^T W^T + V\xi^T. \tag{13}$$

As discussed in the previous section, U and V are pseudoinverse matrices for W and H, respectively, i.e., $UW = I$ and $HV = I$. Models (12) and (13) can thus be reformulated as follows:

$$W^T X = W^T W H + \xi \tag{14}$$
$$H X^T = H H^T W^T + \xi^T. \tag{15}$$

The above models can be further formulated in a uniform as

$$B = A\Phi + \vartheta \tag{16}$$

where, in the case of model (14), $B = W^T X$, $A = W^T W$, $\Phi = H$, and $\vartheta = \xi$, and $B = HX^T$, $A = HH^T$, $\Phi = W^T$, and $\vartheta = \xi^T$ in the case of model (15). In comparison with (1), its purpose is to minimize ξ, while the cost function of (16) minimizes the items of $U^T\xi$ and $V\xi^T$ alternately. Meanwhile, in (16), the nonnegative constraint and the abundance sum-to-one constraint of matrix Φ must be fulfilled.

It is clear that both $W^T W$ and HH^T are *symmetric positive semidefinite* matrices, which means that the model (16) is ill-posed and there does not exist a unique and stable solution. To deal with this problem, an additional auxiliary constraint

on Φ is usually introduced as a regularization term, which can incorporate some prior knowledge and reflect the characteristics of the problem to tackle. However, those methods still suffer from the following drawbacks.

1) The sparse constraint of the cost function is inappropriate, i.e., (11) is equal to minimize $\|\xi\|_F^2 + \lambda\|H\|_q$. However, according to the error analysis of the traditional LMM, we should minimize (9) and (10), respectively.
2) The solution of the sparse equation is nonuniqueness, and the solutions vary with the initial values.
3) The LMM often leads to ill-posed equations, for which the global optima are hard to obtain.

In this letter, we add a damping term to solve this problem. Thus, (16) can be modified to the following form:

$$B = (A + \varpi I)\Phi + \vartheta \tag{17}$$

where ϖ is a given small positive constant and $I \in \Re^{K\times K}$ is an identity matrix. ϖI is called as a damping term, by which $A + \varpi I$ becomes a *symmetric positive definite (SPD)* matrix. Furthermore, the disadvantages of the regularization term are overcome. As a result, (17) can promote an optimal solution. For simplicity, we call the model in (17) as an *NBSUM*.

In following, we use the CG method to solve the model (17).

A. CG Method

The *CG* method was originally developed in the early 1950s by Hestenes and Stiefel [13] for solving a linear system of equations, such as $B = (A + \varpi I)\Phi$, where $A + \varpi I$ is an SPD matrix. Since the CG method is constructed for sparse linear systems in a saddle point form, it has the potential to overcome a common problem with (projected) gradient descent algorithms [14]. In this letter, we use the CG algorithm for the optimization of the coefficient matrix Φ. An iterative method is adopted in this section.

Let Φ_0 be a given initial approximate solution of Φ in (17), and let the initial residual be $\vartheta_0 = B - (A + \varpi I)\Phi_0$. Based on the initial approximation, a sequence of approximations $\Phi_1, \Phi_2, \ldots$ and the corresponding residual matrices $(\vartheta_i) = B - (A + \varpi I)\Phi_i, i = 1, 2, \ldots$, are generated. The CG residual vectors $vec(\vartheta_i)$ are mutually orthogonal, i.e.,

$$(vec(\vartheta_i))^T\, vec(\vartheta_j) = 0$$

where $i \neq j$ and $vec(\cdot)$ is an operator for stacking the column vectors of a matrix into a single column vector. Φ_i could be updated by the CG method under the Krylov subspace [13] iteratively as

$$\Phi_i = \Phi_{i-1} + \alpha_i P_i \tag{18}$$

where P_i is the search direction and α_i denotes the step size. Let $P_0 = \vartheta_0$, and P_i is updated as

$$P_i = \vartheta_i + \beta_i P_{i-1} \tag{19}$$

where

$$\beta_i = \frac{\|\vartheta_i\|_F}{\|\vartheta_{i-1}\|_F} \tag{20}$$

$$\alpha_i = \frac{\|\vartheta_i\|_F^2}{(vec(P_i))^T\, vec(\varpi P_i + AP_i)}. \tag{21}$$

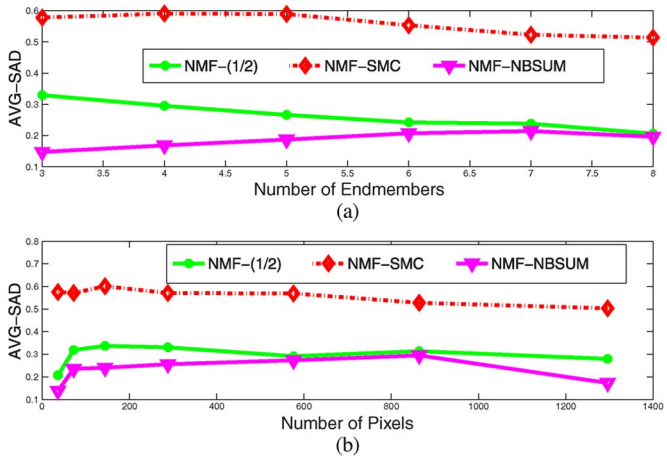

Fig. 1. AVG-SAD values versus (a) number of end-members and (b) number of pixels for the three algorithms.

B. Improved NMF Based on NBSUM

NMF is utilized to calculated matrices W and H. Here, NMF is based on NBSUM, which is tackled by the iteration of the method CG. We denote the improved NMF for blind SU as *NMF-NBSUM*. Generally, we set $constant = 10^{-6}$. Its main procedure can be described as follows.

Step 1) Initialize $W_0 \in R_+^{M\times K}$, $H_0 \in R_+^{K\times N}$, and $\varpi = 10^{-8}$, and set $t = 1$. Rescale each column of H to be a unit norm.
Step 2) Fix W_{t-1}, and optimize H_t by (14) with the CG method.
Step 3) Fix H_t, and optimize W_t by (15) with the CG method.
Step 4) Repeat *Steps 2)* and *3)* until the maximum number of iterations has been reached or $\vartheta < constant$.

IV. Experiments

In this section, we assess the performance of NMF-NBSUM on both synthetic and real data. Four state-of-the-art methods are used for comparison study: vertex component analysis (VCA) [15], NMF-SMC [9], simplex identification via variable splitting and augmented Lagrangian (SISAL) [16], and $L_{1/2}NMF$ [6]. Among them, NMF-SMC and $L_{1/2}NMF$ are based on NMF, while VCA and SISAL are geometric approaches. It should be noted that VCA needs the presence of pure pixels; moreover, VCA and SISAL infer abundances indirectly. In synthetic experiment, the abundances follow a Dirichlet distribution [17], and we just compare NMF-NBSUM with two sparse NMF methods. We use the spectral angel distance (SAD) criteria to evaluate the unmixing results. For the kth end-member, the SAD is defined as

$$SAD_k = \cos^{-1}\frac{\widehat{w_k^T} w_k}{\|\widehat{w_k}\|_2\|w_k\|_2}$$

where w_k and $\widehat{w_k}$ are the resultant and reference end-member signatures, respectively.

A. Experimental Results on Synthetic Data

In order to conduct a comprehensive comparative analysis, a synthetic image is designed and simulated based on the

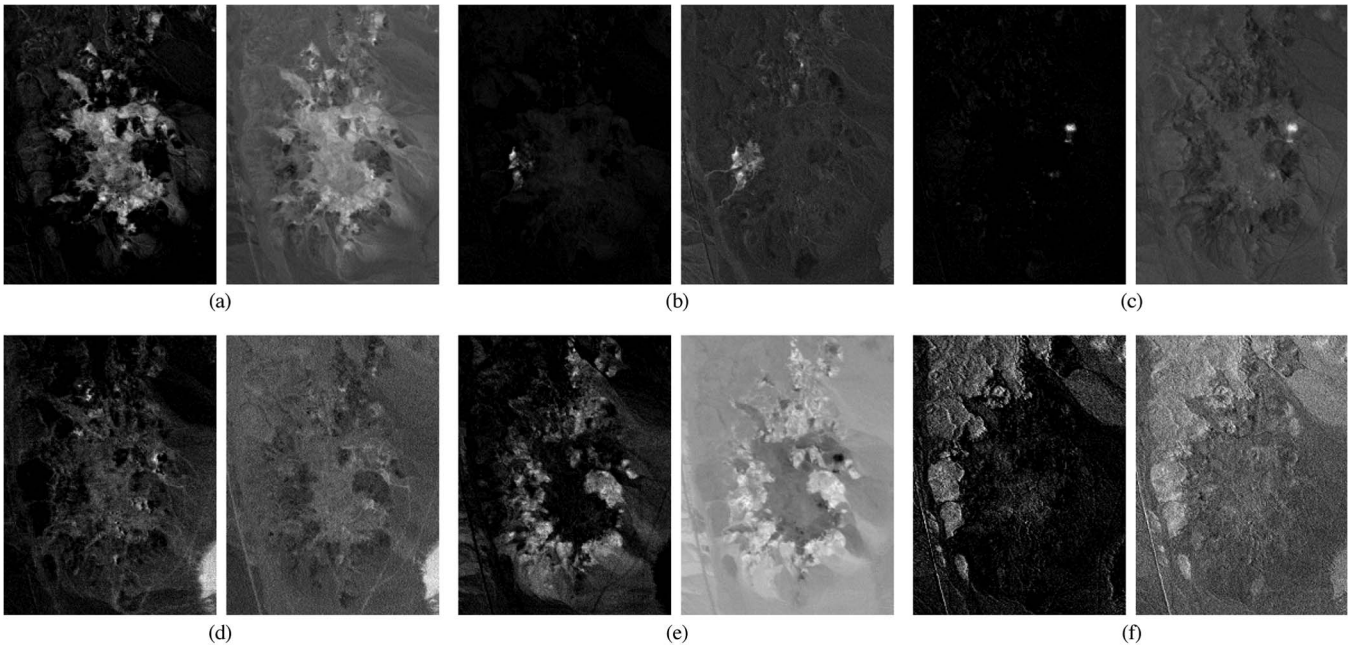

Fig. 2. Corresponding estimations of abundance map obtained by (left) NMF-NBSUM and (right) VCA, respectively. (a) Abundance map of chalcedony. (b) Abundance map of buddingtonite. (c) Abundance map of muscovite. (d) Abundance map of montmorillonite. (e) Abundance map of kaolinite. (f) Abundance map of sphene.

reflectance spectra of the U.S. Geological Survey (USGS) ground-truth mineral spectra.[1] The end-member signature matrix $W_{M\times K}$ is selected from the USGS digital spectral library, and the abundance matrix $H_{K\times N}$ is generated according to a Dirichlet distribution, which is the same as in [17]. To simulate the possible errors and sensor noises, some Gaussian noises are added to the mixtures with a zero mean [17] and a signal-to-noise ratio $SNR = 10\log(E(\chi\chi^T)/E(\epsilon\epsilon^T))$, where χ denotes the real signals and ϵ denotes the corresponding noise. Each run consists of 21 spectra made from K pure materials. The average of SAD is calculated as

$$\text{AVG-SAD} = \frac{1}{K}\sum_{j=1}^{K} SAD_j.$$

First, we fix the number of pixels and noise by setting $N = 1296$ and $SNR = 30$ dB and set the number of end-members as $r = 3$, 4, 5, 6, 7, and 8. The AVG-SAD values versus the number of end-members are plotted in Fig. 1(a). From the figure, we can see that only NMF-NBSUM can obtain the most accurate end-member signatures. When the number of end-members $r = 3$, 4, and 5, the differences from the algorithms are huge.

Second, we fix the number of end-members and noise by setting $R = 3$ and $SNR = 30$ dB and set the number of pixels as $n = 36$, 72, 144, 288, 576, 864, and 1296. Fig. 1(b) shows the AVG-SAD values versus the number of pixels. It is clear that NMF-NBSUM achieves the best performance among the three algorithms.

From the experimental results, we can conclude that NMF-NBSUM overcomes the shortcomings of LMM and increases the probability of finding an optimal solution.

B. Experimental Results on Real Data

In this section, the algorithms are applied to the widely used Cuprite data which were captured by AVIRIS in June 1997 in the state of Nevada.[2] There are 224 bands in the data, covering the wavelength range of 0.37–2.48 m. The spectral resolution is 10 nm. The imaging area is located in the desert about 200 km northwest of Las Vegas, NV, USA, where it is covered by various exposed minerals with a highway (U.S.95) crossing through but not by vegetation. An approximated distribution of the minerals has been illustrated in [18]. The minerals are normally highly mixed. In the experiment, a block of size 250×191 is taken from the original data. Before unmixing, the 1st–2nd, 104th–113th, 148th–167th, and 221st–224th bands are removed as noisy or water-absorption bands, leaving 188 bands left. The initial data are formatted into MAT by the software of MultiSpec.[3] The number of end-members is assigned as 12, using the virtual-dimension method [19].

Fig. 2 shows some resulting abundances of NMF-NBSUM and VCA. As the end-member number is a little large, we mainly compare the abundance maps of seven representative end-members. In the figures, the pure black denotes that the percentage of a certain sort of object in this pixel is 0, while the pure white denotes 1. From the figures, we can see that NMF-NBSUM recovers the abundances more efficiently than VCA (according to available data[4] and an existing analysis of the data set [20]), particularly for end-members, e.g., chalcedony, buddingtonite, muscovite, etc.

We also employ the spectra of corresponding minerals picked up from the USGS library as the reference end-member signatures. In order to evaluate the performances quantitatively, we

[1]The library is available at http://speclab.cr.usgs.gov/spectral.lib04/lib04-AVIRIS.html

[2]available at http://aviris.jpl.nasa.gov/html/aviris.freedata.html

[3]available at http://cobweb.ecn.purdue.edu/biehl/MultiSpec/

[4]available at http://speclab.cr.usgs.gov/cuprite95.tgif.2.2um.map.gif

TABLE I
SAD METRIC VALUES BETWEEN LIBRARY SPECTRUM AND EXTRACTED SPECTRUM OBTAINED BY THE COMPARING METHODS

	NMF-NBSUM	VCA	SISAL	$L_{\frac{1}{2}}$NMF	NMF-SMC
Alunite	0.1640	**0.1035**	0.2589	/	/
Andradite	0.0806	**0.0573**	0.1144	0.4057	0.3860
Montmorillonite	**0.0362**	0.0607	0.1084	0.3529	0.4473
Dumortierite	**0.0814**	0.0922	0.1143	0.3752	0.4100
Buddingtonite	**0.0741**	0.0863	0.1253	0.3655	0.4100
Kaolinite	**0.0582**	0.0692	0.0655	0.4079	0.4349
Desert Varnish	0.0926	**0.0913**	/	/	/
Chalcedony	**0.0712**	0.0715	0.1090	0.3734	0.4564
Nontronite	**0.0801**	0.0972	0.1084	0.3924	0.4228
Sphene	0.0752	**0.0623**	/	0.4226	/
Pyrope	0.0834	**0.0774**	0.1482	0.4047	0.4569
Muscovite	**0.0805**	0.1282	0.1127	0.4003	0.4672
Mean	**0.0815**	0.0831	0.1265	0.3901	0.4324
CPU Time(S)	**3.839**	**1.342**	37.150	5.282	10.361

directly use the results of VCA as the starting points for the NMF-NBSUM learning. The indices SAD_j (calculated using the estimated spectrum from the USGS digital spectral library) of the five algorithms NMF-NBSUM, $L_{1/2}$NMF, NMF-SMC, VCA, and SISAL are shown in Table I. The mean of the SAD_j over ten runs is calculated for these methods. The CPU time is the average time spent per run for unmixing. Based on these results, it can be seen that NMF-NBSUM identifies the most numbers of minerals and gives the best comprehensive result. Moreover, the CPU time of NMF-NBSUM is less than the other two NMF-based methods ($L_{1/2}$NMF and NMF-SMC), although it is not as efficient as the geometric method VCA.

V. CONCLUSION

In this letter, we first analyzed the general LMM model and then proposed a novel blind spectral unmixing method, named NBSUM. The NMF method is employed to deal with the equation, termed as NMF-NBSUM, in which the CG method is used to solve the basic equation. NMF-NBSUM is able to converge more efficiently and the reasons might be the following.

1) The proposed method transforms the LMM into NBSUM which overcomes the limitations of LMM by consideration of both the random measurement error ξ and the pseudoinverse of matrices W and H.
2) The traditional LMM usually leads to ill-posedness, while in our method, a benign equation is constructed to get optimal solution.
3) The CG method is based on the Krylov subspace, and some matrix–matrix operations are avoided.

The proposed approach was applied and compared with some state-of-the-art methods on both the synthetic and the real data. The experimental results show that NMF-NBSUM is promising for blind SU.

REFERENCES

[1] A. Halimi, Y. Altmann, N. Dobigeon, and J.-Y. Tourneret, "Nonlinear unmixing of hyperspectral images using a generalized bilinear model," *IEEE Trans. Geosci. Remote Sens.*, vol. 49, no. 11, pp. 4153–4162, Nov. 2011.

[2] X. Chen, J. Chen, X. Jia, B. Somers, J. Wu, and P. Coppin, "A quantitative analysis of virtual endmembers increased impact on the collinearity effect in spectral unmixing," *IEEE Trans. Geosci. Remote Sens.*, vol. 49, no. 8, pp. 2945–2956, Aug. 2011.

[3] K.-H. Liu, E. Wong, E. Y. Du, C. C.-C. Chen, and C.-I. Chang, "Kernel-based linear spectral mixture analysis," *IEEE Geosci. Remote Sens. Lett.*, vol. 9, no. 1, pp. 129–133, Jan. 2012.

[4] J. M. Bioucas-Dias, A. Plaza, M. Parente, Q. Du, P. Gader, and J. Chanussot, "Hyperspectral unmixing overview: Geometrical, statistical, and sparse regression-based approaches," *IEEE J. Sel. Topics Appl. Earth Observ. Remote Sens.*, vol. 5, no. 2, pp. 354–379, Apr. 2012.

[5] D. D. Lee and H. S. Seung, "Learning the parts of objects by non-negative matrix factorization," *Nature*, vol. 401, no. 6755, pp. 788–791, Oct. 1999.

[6] Y. Qian, J. Z. Sen Jia, and A. Robles-Kelly, "Hyperspectral unmixing via $l_{1/2}$ sparsity-constrained nonnegative matrix factorization," *IEEE Trans. Geosci. Remote Sens.*, vol. 49, no. 11, pp. 4282–4299, Nov. 2011.

[7] L. Miao and H. Qi, "Endmember extraction from highly mixed data using minimum volume constrained nonnegative matrix factorization," *IEEE Trans. Geosci. Remote Sens.*, vol. 45, no. 3, pp. 765–777, Mar. 2007.

[8] X. Liu, L. Z. Wei Xia, and B. Wang, "An approach based on constrained nonnegative matrix factorization to unmix hyperspectral data," *IEEE Trans. Geosci. Remote Sens.*, vol. 49, no. 2, pp. 757–772, Feb. 2011.

[9] Z. Yang, G. Zhou, S. Xie, S. Ding, J.-M. Yang, and J. Zhang, "Blind spectral unmixing based on sparse nonnegative matrix factorization," *IEEE Trans. Geosci. Remote Sens.*, vol. 20, no. 4, pp. 1112–1125, Apr. 2011.

[10] S. Jia and Y. Qian, "Spectral and spatial complexity-based hyperspectral unmixing," *IEEE Trans. Geosci. Remote Sens.*, vol. 45, no. 12, pp. 3867–3879, Dec. 2007.

[11] J. Li, "Wavelet-based feature extraction for improved endmember abundance estimation in linear unmixing of hyperspectral signals," *IEEE Trans. Geosci. Remote Sens.*, vol. 42, no. 3, pp. 644–649, Mar. 2004.

[12] N. Gillis, R. J. Plemmons, and Q. Zhang, "Priors in sparse recursive decompositions of hyperspectral images," in *Proc. SPIE, Algorithms Technol. Multispectr., Hyperspectr. Ultraspectr. Imagery XVIII*, 2012, vol. 8390, p. 83901M.

[13] X. Cai, B. Nielsen, and A. Tveito, "A note on the efficiency of the conjugate gradient method for a class of time-dependent problems," *Numer. Linear Algebra Appl.*, vol. 14, no. 5, pp. 459–467, Jun. 2007.

[14] C. Ding, T. Li, and M. I. Jordan, "Convex and semi-nonnegative matrix factorizations," *IEEE Trans. Pattern Anal. Mach. Intell.*, vol. 32, no. 1, pp. 45–55, Jan. 2010.

[15] J. M. P. Nascimento and J. M. B. Dias, "Vertex component analysis: A fast algorithm to unmix hyperspectral data," *IEEE Trans. Geosci. Remote Sens.*, vol. 43, no. 4, pp. 898–910, Apr. 2005.

[16] J. Bioucas-Dias, "A variable splitting augmented Lagrangian approach to linear spectral unmixing," in *Proc. IEEE Workshop Hyperspectr. Image Signal Process., Evol. Remote Sens.*, 2009, pp. 1–4.

[17] T.-H. Chan, C.-Y. Chi, Y.-M. Huang, and W.-K. Ma, "A convex analysis based minimum-volume enclosing simplex algorithm for hyperspectral unmixing," *IEEE Trans. Signal Process.*, vol. 57, no. 11, pp. 4418–4432, Nov. 2009.

[18] R. N. Clark and G. A. Swayze, "Evolution in imaging spectroscopy analysis and sensor signal-to-noise: An examination of how far we have come," in *Proc. 6th Annu. JPL Airborne Earth Sci. Workshop*, 1996, pp. 49–53.

[19] C.-I. Chang and Q. Du, "Estimation of number of spectrally distinct signal sources in hyperspectral imagery," *IEEE Trans. Geosci. Remote Sens.*, vol. 42, no. 3, pp. 608–619, Mar. 2004.

[20] X. Tao, B. Wang, and L. Zhang, "Orthogonal bases approach for the decomposition of mixed pixels in hyperspectral imagery," *IEEE Geosci. Remote Sens. Lett.*, vol. 6, no. 2, pp. 219–223, Apr. 2009.